

# Single crystal growth and superconductivity in RbNi<sub>2</sub>Se<sub>2</sub>

Hui Liu,<sup>1</sup> Xunwu Hu,<sup>1</sup> Hanjie Guo,<sup>2</sup> Xiao-Kun Teng,<sup>3</sup> Huanpeng Bu,<sup>2</sup> Zhihui Luo,<sup>1</sup>  
Lisi Li,<sup>1</sup> Zengjia Liu,<sup>1</sup> Mengwu Huo,<sup>1</sup> Feixiang Liang,<sup>1</sup> Hualei Sun,<sup>1</sup> Bing Shen,<sup>1</sup>  
Pengcheng Dai,<sup>3</sup> Robert J. Birgeneau,<sup>4,5</sup> Dao-Xin Yao,<sup>1</sup> Ming Yi,<sup>3</sup> and Meng Wang<sup>1,\*</sup>

<sup>1</sup>Center for Neutron Science and Technology, Guangdong Provincial Key Laboratory of Magnetoelectric Physics and Devices, School of Physics, Sun Yat-Sen University, Guangzhou, 510275, China

<sup>2</sup>Neutron Science Platform, Songshan Lake Materials Laboratory, Dongguan, Guangdong, 523808, China

<sup>3</sup>Department of Physics and Astronomy, Rice University, Houston, TX 77005, USA

<sup>4</sup>Department of Physics, University of California, Berkeley, California 94720, USA

<sup>5</sup>Materials Science Division, Lawrence Berkeley National Laboratory, Berkeley, California 94720, USA

We report the synthesis and characterization of RbNi<sub>2</sub>Se<sub>2</sub>, an analog of the iron chalcogenide superconductor Rb<sub>x</sub>Fe<sub>2</sub>Se<sub>2</sub>, via transport, angle resolved photoemission spectroscopy, and density functional theory calculations. A superconducting transition at  $T_c = 1.20$  K is identified. In normal state, RbNi<sub>2</sub>Se<sub>2</sub> shows paramagnetic and Fermi liquid behaviors. A large Sommerfeld coefficient yields a heavy effective electron mass of  $m^* \approx 6m_e$ . In the superconducting state, zero-field electronic specific-heat data  $C_{es}$  can be described by a two-gap BCS model, indicating that RbNi<sub>2</sub>Se<sub>2</sub> is a multi-gap superconductor. Our density functional theory calculations and angle resolved photoemission spectroscopy measurements demonstrate that RbNi<sub>2</sub>Se<sub>2</sub> exhibits relatively weak correlations and multi-band characteristics, consistent with the multi-gap superconductivity.

PACS numbers:

## I. INTRODUCTION

Since the discovery of copper oxide superconductors, researchers have extensively searched for superconductivity in materials with transition metals<sup>1,2</sup>. Significant progress has been made in iron pnictide and chalcogenide compounds, where several structural systems have been identified with the highest  $T_c$  of 55 K achieved in LaFeAsO<sup>3</sup>. Superconductivity was also observed in the compounds consisting of Cr and Mn under pressure, such as CrAs, KCrAs, and MnP<sup>4-6</sup>. Among all of them, superconductivity has been found to be in the vicinity of an antiferromagnetic (AF) order, suggesting that spin fluctuations may play an important role in the mechanism of superconductivity. Nickel oxide materials have analogous structures with copper oxide superconductors. Superconductivity with  $T_c = 9 - 15$  K has also been observed in films of nickel-based compounds<sup>7,8</sup>.

ANi<sub>2</sub>Se<sub>2</sub> ( $A = \text{K, Cs, and Tl}$ ) crystalizes in the ThCr<sub>2</sub>Si<sub>2</sub> structure and shows metallic behavior and Pauli paramagnetism. At low temperatures, superconductivity emerges with the superconducting (SC) transition temperatures of  $T_c \approx 0.8$  K for KNi<sub>2</sub>Se<sub>2</sub> polycrystals, 2.7 K for CsNi<sub>2</sub>Se<sub>2</sub>, and 3.7 K for TlNi<sub>2</sub>Se<sub>2</sub> single crystals<sup>9-11</sup>. While K<sub>0.95</sub>Ni<sub>1.86</sub>Se<sub>2</sub> single crystals do not show superconductivity down to 0.3 K, yielding that the superconductivity is sensitive to the stoichiometry of the samples<sup>12</sup>. As a comparison,  $A_x\text{Fe}_2\text{Se}_2$  system exhibits  $T_c$ s ranging from 20 – 30 K. With different amount of iron vacancies,  $A_x\text{Fe}_{2-\delta}\text{Se}_2$  exhibits a variety of AF orders and iron vacancy orders<sup>13-16</sup>. The replacement of Fe by Co suppresses the superconductivity and induces a ferromagnetic (FM) order in RbCo<sub>2</sub>Se<sub>2</sub><sup>17,18</sup>. The ANi<sub>2</sub>Se<sub>2</sub> superconductors with a formal valence of Ni<sup>1.5+</sup> have been revealed to exhibit remarkable properties. In partic-

ular, they usually exhibit a large Sommerfeld coefficient  $\gamma$ , suggesting a large density of states and unconventional pairing at low temperature<sup>10,11</sup>. One possibility that was proposed was that the large Sommerfeld coefficient might be induced by local charge order<sup>9</sup>. However, angle resolved photoemission spectroscopy (ARPES) measurements yield weak electronic correlations in KNi<sub>2</sub>Se<sub>2</sub> and the origin of the large Sommerfeld coefficient may be driven by the large density states and the Van Hove singularity in the vicinity of the Fermi energy<sup>19</sup>.

In this work, we report the successful synthesis and characterization of RbNi<sub>2</sub>Se<sub>2</sub> single crystals. The crystal structure, electronic band structure, and transport properties have been investigated. We find that RbNi<sub>2</sub>Se<sub>2</sub> is a Pauli paramagnetism and exhibits a SC transition at  $T_c = 1.20$  K. Normal-state specific heat measurements suggest an effective electronic mass enhancement with  $m^* \approx 6m_e$ . In SC state, a two-gap BCS model can match well with the zero-field electronic specific heat, indicating that RbNi<sub>2</sub>Se<sub>2</sub> is a multi-gap superconductor. Comparison with the density functional theory (DFT) calculations and ARPES measurements reveals that RbNi<sub>2</sub>Se<sub>2</sub> is a weakly correlated superconductor with multi bands crossing the Fermi level.

## II. EXPERIMENTAL AND CALCULATION DETAILS

Single crystals of RbNi<sub>2</sub>Se<sub>2</sub> were grown by the self-flux method. First, the precursor NiSe was prepared by heating Ni powders and Se pellets at 500°C. Then, NiSe powders and Rb were put into alumina crucibles according to stoichiometry and sealed in an evacuated silica tube. The mixture was kept at 150°C for 5 h, then heated to 760°C

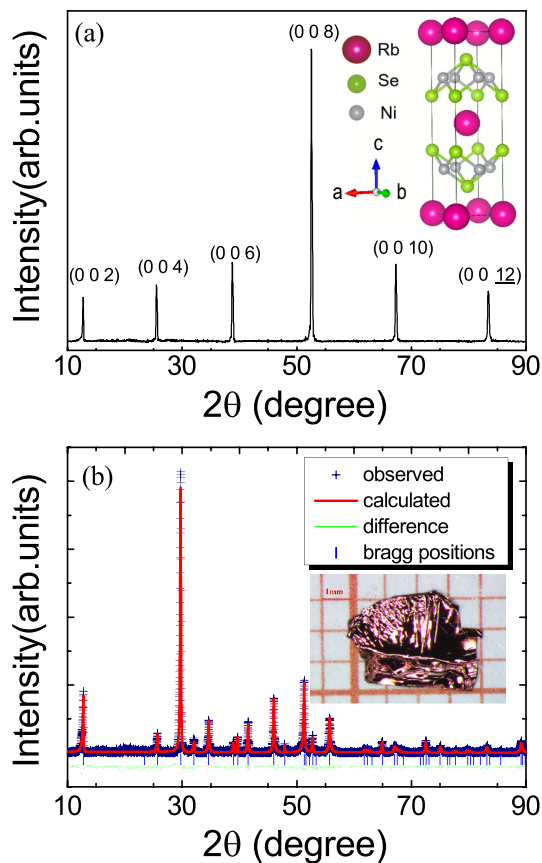


FIG. 1: (a) XRD measurement on the  $ab$  plane of  $\text{RbNi}_2\text{Se}_2$  single crystal. The inset shows the crystal structure. The pink, green, and gray balls represent Rb, Se, and Ni ions. (b) A pattern of XRD measured on powder samples. The inset is a photo of  $\text{RbNi}_2\text{Se}_2$  single crystal.

in 40 h and kept for 5 h, after that heated to  $1050^\circ\text{C}$  in 40 h and held for 5 h. Finally, the temperature was cooled down to  $700^\circ\text{C}$  at a rate of  $3.5^\circ\text{C}/\text{h}$ . To prevent the reaction of Rb with water and air, all of the processes were conducted in an argon-filled glove box. Shiny plate-like single crystals with a typical size of  $4 \times 5 \times 1 \text{ mm}^3$  were grown as shown in the inset of Fig. 1(b).

Single crystal x-ray diffraction (XRD) were conducted on a SuperNova (Rigaku) x-ray diffractometer. The sample was blown by  $\text{N}_2$  during the data collection to avoid exposure to air. The elemental analysis was measured by using an energy-dispersive x-ray spectroscopy (EDS) (EVO, Zeiss). Electrical transport, magnetic and specific heat measurements were performed on a physical property measurement system (PPMS, Quantum Design). The in-plane resistivity  $\rho_{ab}(T)$  was measured using the standard four-probe method on a rectangular sheet crystal to keep current flowing in the  $ab$ -plane. The Vienna *Ab initio* Simulation Package (VASP) was employed for the DFT calculations<sup>20</sup>. ARPES measurements were performed on a helium-lamp based system with a DA30 electron analyzer. Single crystals were cleaved *in-situ* in ultra-high vacuum with a base pressure better than

TABLE I: Single-crystal of  $\text{RbNi}_2\text{Se}_2$  refinement at 150 K.

Formula weight	223.14
Crystal system	Tetragonal
Space group	I4/mmm
Unit-cell parameters	$a = b = 3.9272(3) \text{ \AA}$ $c = 13.8650(5) \text{ \AA}$ $\alpha = \beta = \gamma = 90^\circ$
Atomic parameters	
Rb	$2b(0,0,1/2)$
Ni	$4d(0,1/2,3/4)$
Se	$4e(1/2,1/2,0.6502(1))$
Density	$3.466 \text{ g/cm}^3$
F(000)	198
Radiation	Mo $K\alpha$ ( $\lambda = 0.7107 \text{ \AA}$ )
$2\theta$ for data collection	$10.794^\circ$ to $60.562^\circ$
Index ranges	$-4 \leq h \leq 5, -5 \leq k \leq 5,$ $-11 \leq l \leq 18$
Reflections collected	808
Independent reflections	119
Data/restraints/parameters	119/0/5
Goodness-of-fit on $F^2$	1.204
Final R indexes [ $I \geq 2\sigma(I)$ ]	$R_1 = 0.0378, wR_2 = 0.1001$
Largest diff. peak/hole/ $e \text{ \AA}^{-3}$	$3.06/-2.04$

$5 \times 10^{-11}$  Torr at 30 K. Energy and angular resolutions were better than 20 meV and  $0.1^\circ$ , respectively.

### III. RESULTS AND DISCUSSIONS

All peaks from single crystal XRD can be indexed with the  $\text{ThCr}_2\text{Si}_2$ -type structure (space group: I4/mmm), which is illustrated in the inset of Fig. 1(a). The determined lattice parameters are  $a = b = 3.9272(3)$ , and  $c = 13.8650(5) \text{ \AA}$  at 150 K with the volume of unit cell between that of  $\text{KNi}_2\text{Se}_2$  and  $\text{CsNi}_2\text{Se}_2$ . Details of the atom coordinates and other key information are shown in Table I. To show the quality of the samples, we present a  $\theta-2\theta$  scan of a single crystal along the ( $H = 0, K = 0, L$ ) in Fig. 1(a) and an XRD pattern on a powder sample in Fig. 1(b), where ( $H, K, L$ ) are Miller indices in reciprocal lattice units. No peaks from impurity could be identified. The EDS results for several single crystals are rather homogenous and the determined average atomic ratios are  $\text{Rb}:\text{Ni}:\text{Se} = 1.16(4):2.04(3):2.00(6)$  when the content of Se is normalized to be 2, close to the stoichiometry of  $\text{RbNi}_2\text{Se}_2$ .

Temperature dependence of the resistivity for  $\text{RbNi}_2\text{Se}_2$  is shown in Fig. 2(a). The electric current is applied in the  $ab$ -plane. The value of  $\rho_{ab}$  is about  $92.1 \mu\Omega\text{-cm}$  at 300 K and only about  $1.5 \mu\Omega\text{-cm}$  at 1.8 K. The residual resistivity ratio ( $RRR$ ) of 61.4 [ $\rho_{ab}(300 \text{ K})/\rho_{ab}(1.8 \text{ K})$ ] suggests remarkable metallicity

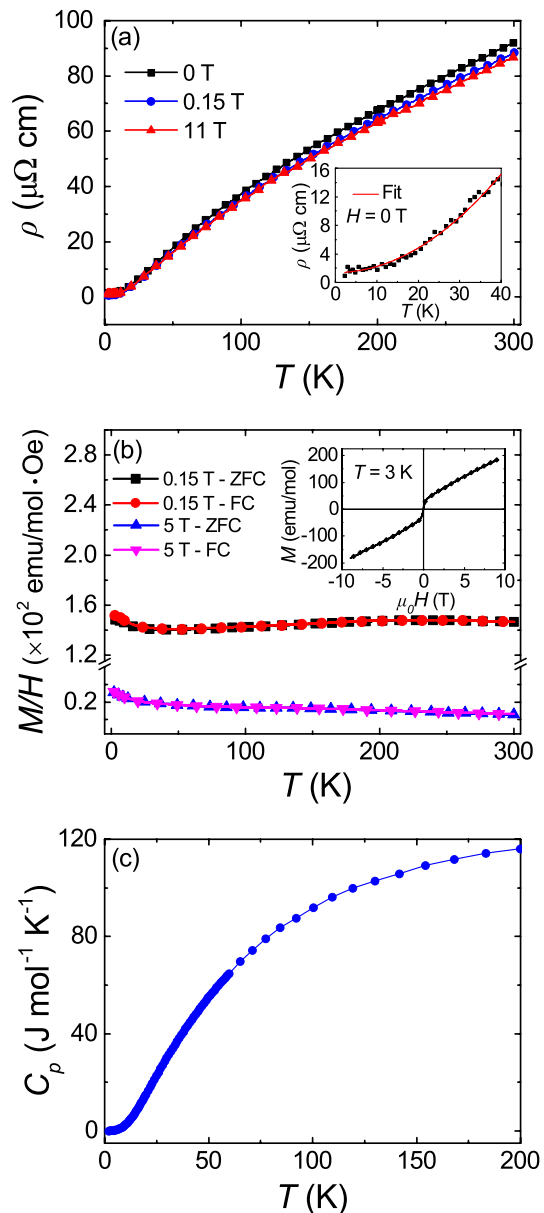


FIG. 2: (a) Temperature dependence of in-plane resistivity  $\rho_{ab}(T)$  with magnetic fields  $H = 0, 0.15,$  and  $11$  T along the  $c$  axis. The inset shows the fitted result using  $\rho_{ab}(T) = \rho_0 + AT^2$  from  $1.8$  to  $40$  K. The red line is a fitting curve. (b) Temperature dependence of ZFC and FC magnetic susceptibility with applying various external magnetic fields along the  $c$  axis. The inset shows a magnetization hysteresis loop at  $3$  K. (c) Temperature dependence of  $C_p(T)$  from  $2$  to  $300$  K.

and high quality of the single crystals<sup>12,21,22</sup>. The resistivity measured at  $0, 0.15,$  and  $11$  T shows a metallic behavior without any anomaly or strong magnetic field dependence. The resistivity  $\rho_{ab}$  below  $40$  K can be well described by the equation  $\rho_{ab}(T) = \rho_0 + AT^2$  as shown in the inset of Fig. 2(a), where  $\rho_0 = 1.211 \mu\Omega\text{-cm}$  and  $A = 0.012 \mu\Omega\text{-cm}/\text{K}^2$ , revealing a paramagnetic Fermi liquid behavior<sup>23</sup>. The magnetic susceptibility

is nearly independent of temperature, yielding a Pauli paramagnetic behaviour as shown in Fig. 2(b). A weak FM sign is revealed from the hysteresis loop shown in the inset of Fig. 2(b), which could be ascribed to a small amount of Ni impurity<sup>24</sup>. The specific heat from  $2$  to  $200$  K shown in Fig. 2(c) also suggests that no phase transition occurs in this temperature range.

To explore the possible superconductivity, we show measurements down to  $50$  mK in Fig. 3. The magnetic susceptibility at low temperatures is shown in Fig. 3(a). A clear diamagnetic response appears below  $1.20$  K under zero field, indicating a SC transition. The transition shifts to lower temperatures with an increase of the  $dc$  bias field, consistent with the Meissner effect of superconductivity. With knowing  $T_c \approx 0.8$  K for  $\text{KNi}_2\text{Se}_2$ <sup>9</sup> and  $T_c \approx 2.7$  K for  $\text{CsNi}_2\text{Se}_2$ <sup>10</sup>, the diamagnetic response at  $1.20$  K should correspond to the SC transition of  $\text{RbNi}_2\text{Se}_2$ . We plot the onset SC transition temperatures at various magnetic fields and fit the upper critical field  $\mu_0 H_{c2}(0)$  using the Ginzburg-Landau theory with the formula  $\mu_0 H_{c2}(T) = \mu_0 H_{c2}(0) \times (1 - t^2)/(1 + t^2)$ , where  $t$  is the reduced temperature  $t = T/T_c$ . As shown in Fig. 3(b), the resultant  $\mu_0 H_{c2}(0) = 1.38$  T is within the Pauli limit,  $\mu_0 H_{c2}^p(0) = 2.37$  T, indicating a weak coupling behavior<sup>25</sup>.

stop here

Figure 3(c) displays the specific heat measured at low temperatures. In normal state, a fit to the specific heat  $C_p$  from  $1.5$  to  $3.8$  K using  $C_p/T = \gamma_N + \beta T^2$  results in the Sommerfeld coefficient  $\gamma_N = 30.30 \text{ mJ}\cdot\text{mol}^{-1}\text{K}^{-2}$  and  $\beta = 3.67 \text{ mJ}\cdot\text{mol}^{-1}\text{K}^{-4}$ , as shown in the inset. The Debye temperature  $\Theta_D$  is estimated to be of  $167$  K from the equation  $\Theta_D = (12\pi^4 NR/5\beta)^{1/3}$ , where  $N = 5$  is the atomic number in each formula unit and  $R$  is the ideal gas constant. The  $\gamma_N$  for  $\text{RbNi}_2\text{Se}_2$  is comparable with that of  $\text{KNi}_2\text{Se}_2$  ( $\sim 44 \text{ mJ}\cdot\text{mol}^{-1}\text{K}^{-2}$ )<sup>9</sup>,  $\text{CsNi}_2\text{Se}_2$  ( $\sim 77 \text{ mJ}\cdot\text{mol}^{-1}\text{K}^{-2}$ )<sup>10</sup>, and  $\text{TiNi}_2\text{Se}_2$  ( $\sim 40 \text{ mJ}\cdot\text{mol}^{-1}\text{K}^{-2}$ )<sup>11</sup>. The effective mass of electrons  $m^*$  can be estimated through Eq. 1<sup>26</sup>:

$$m^* = \hbar^2 k_F^2 \gamma_N / \pi^2 n k_B^2 \quad (1)$$

where  $k_B$  is the Boltzmann constant and the carrier density  $n$  is calculated by the number of electrons ( $Z$ ) per cell volume ( $V$ ). Using a spherical Fermi surface approximation, the Fermi wave vector can be estimated by  $k_F = (3\pi^2 n)^{1/3}$ . Assuming that Ni contributes  $1.5$  electrons ( $Z = 6$ ), we obtain  $k_F = 9.4 \times 10^9 \text{ m}^{-1}$ . The estimated effective mass of electrons  $m^*/m_e = 6$  for  $\text{RbNi}_2\text{Se}_2$  is significantly enhanced compared with the bare electron mass  $m_e$ . Combining the parameters from fitting the electronic specific heat and the quadratic temperature dependent regime of resistivity, the Kadowaki-Woods ratio,  $A/\gamma_N^2$ , is calculated to be  $0.94 \times 10^{-5} \mu\Omega\text{-cm}(\text{mol}\cdot\text{K}^2\text{mJ})^2$ , close to  $\sim 10^{-5} \mu\Omega\text{-cm}(\text{mol}\cdot\text{K}^2\text{mJ})^2$  of heavy fermion systems<sup>27</sup>. This scaling relation yields  $\text{RbNi}_2\text{Se}_2$  with the heavy-fermion behavior.

In SC state, the specific heat data reveals a clear  $\lambda$ -anomaly under zero field with a maximum at  $0.94$  K [Fig.

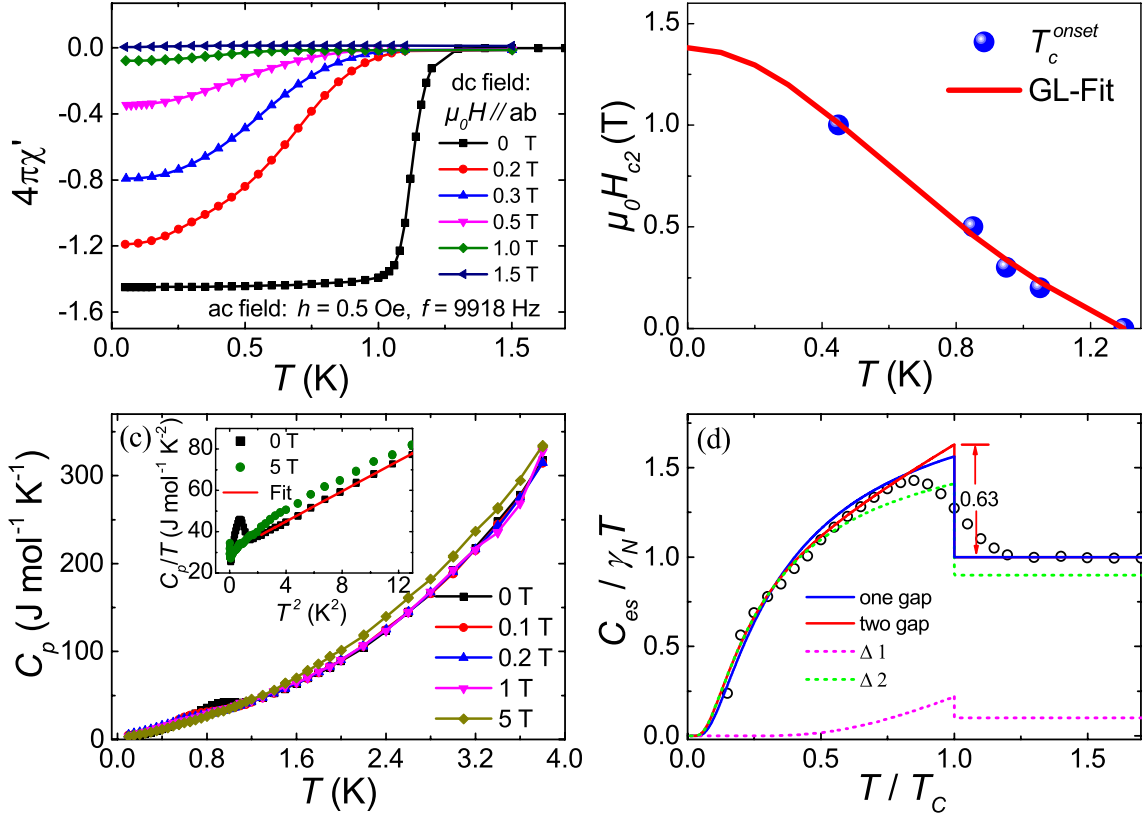


FIG. 3: (a) Diamagnetization of superconductivity under various magnetic fields. (b) Upper critical field  $H_{c2}$ , as a function of temperature. The red solid line shows a fit with the Ginzburg-Landau expression as discussed in the text. (c) The low-temperature specific heat of  $\text{RbNi}_2\text{Se}_2$ , measured at various fields near superconducting transition. The inset shows the Schottky anomaly at zero field and 5 T and a fitting of  $C_p$  in normal state. (d) Reduced temperature  $T/T_c$  dependence of electronic specific heat divided by temperature and  $\gamma_N$ ,  $C_{es}/\gamma_N T$ , in the SC state at zero field, where  $C_{es} = C_p - C_{lattice} - C_N$ . The two solid lines show the fitting curves of the one-gap BCS model and the two-gap model to  $C_{es}/\gamma_N T$ , respectively. The dashed lines show the contributions from two different gaps,  $\Delta_1$  and  $\Delta_2$ , respectively.

3(c)], suggesting bulk superconductivity. Applying an external magnetic field, the SC transition moves quickly to lower temperatures. As shown in the inset of Fig. 3(c), an upturn appears on  $C_p/T$  below  $T^2 < 0.1 \text{ K}^2$ . The small upturn could be described by the Schottky anomaly for paramagnetic impurity spins<sup>9</sup>, which can be well fitted by  $C_N = D(H)T^{-2}$  with  $D(H=0) = 0.07 \text{ mJ}\cdot\text{K}\cdot\text{mol}^{-1}$ .

In order to get information about the SC gap, we extract the electronic specific heat  $C_{es}$  by subtracting the phonon contribution  $C_{lattice}$  and Schottky anomaly  $C_N$  from the total  $C_p$ ,  $C_{es} = C_p - C_{lattice} - C_N$ . The electronic specific heat data  $C_{es}/(\gamma_N T)$  against  $T/T_c$  are shown in Fig. 3(d), where  $\gamma_N$  has been revealed in the normal state. The  $T_c$  is determined to be 0.94 K using an equal-area entropy construction. The heat jump at transition is 0.63, smaller than that of the theoretical value of 1.43 in the BCS weak-coupling scenario<sup>28</sup>. We employ both one-gap and two-gap BCS models  $C_{es} = \sum C_i \exp(-\Delta_i/k_B T)$  to fit the electronic specific heat, where  $\Delta_i$  is the size of the  $i^{\text{th}}$  SC gap at 0 K. The one-gap model reveals  $\Delta_0/k_B T_c = 0.30$  that is smaller than

the value of 1.76 in the BCS theory<sup>29</sup>. In the two-gap model, the total specific heat can be considered as the sum of electronic contributions from two bands. Our fitting yields the sizes of two gaps of  $\Delta_1/k_B T_c = 2.51$  and  $\Delta_2/k_B T_c = 0.25$ , respectively. The ratio of the contributions from the two gaps is  $\sim 1.5 : 1$  as presented by the dashed lines in Fig. 3(d). The better fitting using the two-gap model indicates that  $\text{RbNi}_2\text{Se}_2$  may be a multi-gap superconductor.

The electron-phonon coupling strength is also calculated by employing the inverted McMillan formula<sup>30</sup>:

$$\lambda_{ep} = \frac{1.04 + \mu^* \ln(\Theta_D/1.45T_c)}{(1 - 0.62\mu^*) \ln(\Theta_D/1.45T_c) - 1.04} \quad (2)$$

where  $\mu^*$  represents the Coulomb repulsion pseudopotential, which we adopt  $\mu^* = 0.13$  for this system<sup>31</sup>. Generally, the  $\lambda_{ep}$  for strongly coupled superconductors are close to 1, and  $\lambda_{ep} \rightarrow 0.5$  is viewed as weak coupled superconductors<sup>30</sup>. The  $\lambda_{ep}$  for  $\text{RbNi}_2\text{Se}_2$  is 0.49, suggesting that  $\text{RbNi}_2\text{Se}_2$  is a weakly coupled superconductor, consistent with the specific heat analysis.

To check the multi-band character, we conducted DFT

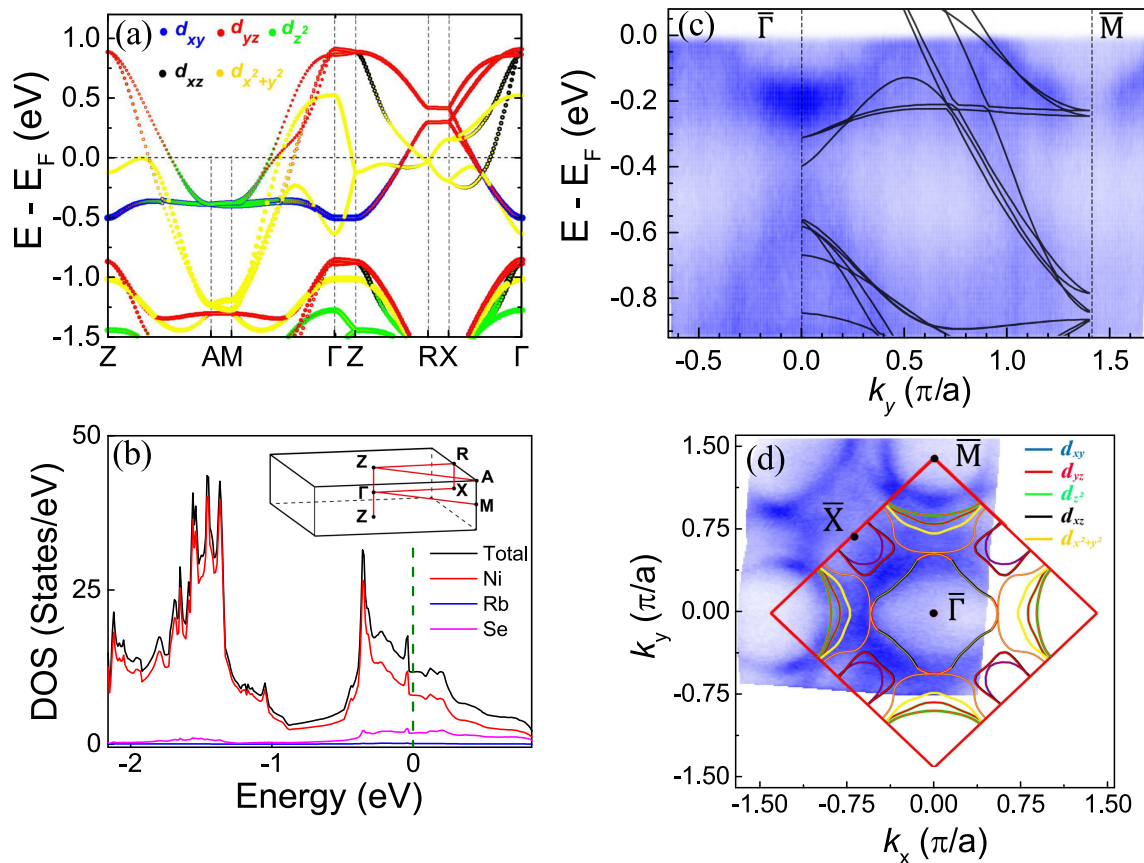


FIG. 4: (a) Projected band structure of Ni 3d in RbNi<sub>2</sub>Se<sub>2</sub>. Colors of the circle represent the different nickel orbitals, and the weight of each orbital is displayed by the size of the circles. The dashed lines are guide to eyes. (b) Density of states (DOS) near the Fermi level of RbNi<sub>2</sub>Se<sub>2</sub>. The red, blue and purple curves represent contributions from Ni, Rb and Se, respectively. Inset: The coordinates of the high symmetry  $\mathbf{k}$ -path in reciprocal space of the tetragonal unit cell. (c) Measured spectral images along the high symmetry direction  $\Gamma \sim M$ . The black lines are band structure calculated by the DFT. (d) The Fermi surface mapping at 35 K with the Brillouin zone (BZ) marked by a red square.

calculations and ARPES measurements on the electronic band structure. Figures 4(a) and 4(b) show the calculated electronic bands of Ni ions and the integrated density of states of Ni, Rb, and Se. The electronic states near the Fermi surface are governed by the 3d orbitals of Ni ions. In Fig 4(c), the measured electronic structure of RbNi<sub>2</sub>Se<sub>2</sub> is compared with the band structure obtained from the DFT calculations. The calculated curves (black lines) are scaled and overlaid onto the photoemission intensity along the  $\Gamma - M$  direction. The theoretical and experimental data match qualitatively with a renormalization factor of about 1.8. This factor is relatively small compared to other iron-based superconductors<sup>32</sup>, indicating that the electronic correlations are moderate. The moderate correlations suggest that the superconductivity is most likely originated from the electron-phonon coupling, similar to the two-gap superconductor MgB<sub>2</sub><sup>33,34</sup>. Figure 4(d) shows the photoemission intensity map of the Fermi surface, overlaid with the DFT calculated Fermi surfaces. The multiple Fermi pockets observed are consistent with the multi-band behavior of this compound, reinforcing the condition for the two-gap

feature in the SC state. The band structure is reminiscent of the closely-related compound RbCo<sub>2</sub>Se<sub>2</sub><sup>18</sup>. However, the 3d<sub>x<sup>2</sup>+y<sup>2</sup></sub> flat band that induces itinerant ferromagnetism in RbCo<sub>2</sub>Se<sub>2</sub> is observed here to be well below the Fermi level, due to the electron doping resulted from the replacement of Co by Ni.

As ANi<sub>2</sub>Se<sub>2</sub> ( $A = \text{K, Cs, and Tl}$ ) superconductors, RbNi<sub>2</sub>Se<sub>2</sub> also exhibits an enhanced effective electron mass with a large Sommerfeld coefficient from specific heat. However, ARPES data reveal that the electronic correlation is not strong. To understand the reason of the large Sommerfeld coefficient,  $\gamma$  is estimated with  $\lambda_{ep}$  and  $N(0)$  at the Fermi level through the relationship<sup>35</sup>:

$$\gamma = \frac{\pi^2 k_B^2 N(E_F)(1 + \lambda_{ep})}{3} \quad (3)$$

From the DOS in Fig. 4(b),  $N(E_F)$  is estimated to be 11.68 states/eV per formula, resulting in  $\gamma = 40.98 \text{ mJ}\cdot\text{mol}^{-1}\text{K}^{-2}$  that is close to the experimental value of  $30.30 \text{ mJ}\cdot\text{mol}^{-1}\text{K}^{-2}$ . Therefore, the result suggests that the large  $\gamma_N$  is related to the large DOS at the Fermi level as proposed in KNi<sub>2</sub>Se<sub>2</sub><sup>19</sup>, instead of the heavy fermion

state. For  $\text{ANi}_2\text{Se}_2$  ( $A = \text{K}, \text{Rb}, \text{and Cs}$ ), the increase of the atomic radiuses of alkali metals works as applying a pressure to the Ni-Se layers. The DOS of Ni  $3d$  orbitals at the Fermi surface, the Sommerfeld coefficient  $\gamma_N$ , and the electronic correlations are all enhanced. In the framework of the BCS theory, the SC transition temperature  $T_c$  increases accordingly, as the experimental observations in  $\text{KNi}_2\text{Se}_2$ ,  $\text{RbNi}_2\text{Se}_2$ , and  $\text{CsNi}_2\text{Se}_2$ <sup>9-11</sup>.

#### IV. SUMMARY

In summary, we have successfully synthesized single crystals of  $\text{RbNi}_2\text{Se}_2$  and characterized the physical properties.  $\text{RbNi}_2\text{Se}_2$  is found to be a weakly coupled superconductor with  $T_c = 1.2$  K. In normal state,  $\text{RbNi}_2\text{Se}_2$  exhibits Fermi liquid behavior and Pauli paramagnetism. In the SC state, the zero-field electronic specific heat can be well described with a two-gap BCS model, indicating that  $\text{RbNi}_2\text{Se}_2$  possesses multi-gap feature. DFT calculations and ARPES measurements demonstrate that multi electronic bands of the  $3d$  orbitals of Ni ions cross the Fermi level. Our analyses reveal that the large Sommerfeld coefficient of  $\text{RbNi}_2\text{Se}_2$  is originated from the large

DOS at the Fermi surface.

#### V. ACKNOWLEDGMENTS

We thank Shiliang Li for fruitful discussions. Work at Sun Yat-Sen University was supported by the National Natural Science Foundation of China (Grants No. 12174454, 11904414, 11904416, 11974432, U2130101), the Guangdong Basic and Applied Basic Research Foundation (No. 2021B1515120015), National Key Research and Development Program of China (No. 2019YFA0705702, 2018YFA0306001, 2017YFA0206203), and GBABRF-2019A1515011337. Work at SLAB was supported by NSF of China with Grant No. 12004270, and GBABR-2019A1515110517. ARPES work at Rice is supported by the Robert A. Welch Foundation Grant No. C-2024 (M. Y.). P. D. is also supported by US Department of Energy, BES under Grant No. DE-SC0012311. Work at Berkeley was funded by the U.S. Department of Energy, Office of Science, Office of Basic Energy Sciences, Materials Sciences and Engineering Division under Contract No. DE-AC02-05-CH11231 (Quantum Materials program KC2202).

\* Electronic address: [wangmeng5@mail.sysu.edu.cn](mailto:wangmeng5@mail.sysu.edu.cn)

- <sup>1</sup> J. G. Bednorz, M. Takashige, and K. A. Müller, *Europhys. Lett.* **3**, 379 (1987), URL <http://link.springer.com/10.1007/BF01303701>.
- <sup>2</sup> K. Takada, H. Sakurai, E. Takayama-Muromachi, F. Izumi, R. A. Dilanian, and T. Sasaki, *Nature* **422**, 53 (2003), ISSN 0028-0836, URL <http://www.nature.com/articles/nature01450>.
- <sup>3</sup> Z.-A. Ren, G.-C. Che, X.-L. Dong, J. Yang, W. Lu, W. Yi, X.-L. Shen, Z.-C. Li, L.-L. Sun, F. Zhou, et al., *EPL (Europhysics Lett.)* **83**, 17002 (2008), ISSN 0295-5075, URL <https://iopscience.iop.org/article/10.1209/0295-5075/83/17002>.
- <sup>4</sup> W. Wu, J. Cheng, K. Matsubayashi, P. Kong, F. Lin, C. Jin, N. Wang, Y. Uwatoko, and J. Luo, *Nat. Commun.* **5**, 5508 (2014), ISSN 2041-1723, URL <http://dx.doi.org/10.1038/ncomms6508><http://www.nature.com/articles/ncomms6508>.
- <sup>5</sup> Q.-G. Mu, B.-B. Ruan, B.-J. Pan, T. Liu, J. Yu, K. Zhao, G.-F. Chen, and Z.-A. Ren, *Phys. Rev. B* **96**, 140504 (2017), ISSN 2469-9950, URL <https://link.aps.org/doi/10.1103/PhysRevB.96.140504>.
- <sup>6</sup> J.-G. Cheng, K. Matsubayashi, W. Wu, J. P. Sun, F. K. Lin, J. L. Luo, and Y. Uwatoko, *Phys. Rev. Lett.* **114**, 117001 (2015), ISSN 0031-9007, URL <https://link.aps.org/doi/10.1103/PhysRevLett.114.117001>.
- <sup>7</sup> D. Li, K. Lee, B. Y. Wang, M. Osada, S. Crossley, H. R. Lee, Y. Cui, Y. Hikita, and H. Y. Hwang, *Nature* **572**, 624 (2019), ISSN 0028-0836, URL <http://dx.doi.org/10.1038/s41586-019-1496-5><http://www.nature.com/articles/s41586-019-1496-5>.
- <sup>8</sup> Q. Gu and H.-H. Wen, *Innov.* **3**, 100202 (2022), ISSN 26666758.

- <sup>9</sup> J. R. Neilson, A. Llobet, A. V. Stier, L. Wu, J. Wen, J. Tao, Y. Zhu, Z. B. Tesanovic, N. P. Armitage, and T. M. McQueen, *Phys. Rev. B* **86**, 054512 (2012), ISSN 1098-0121, URL <https://link.aps.org/doi/10.1103/PhysRevB.86.054512>.
- <sup>10</sup> Chen, Huimin and Yang, Jinhu and Cao, Chao and Li, Lin and Su, Qiping and Chen, Bin and Wang, Hangdong and Mao, Qianhui and Xu, Binjie and Du, Jianhua and Fang, Minghu, *Supercond. Sci. Technol.* **29**, 045008 (2016), URL <https://iopscience.iop.org/article/10.1088/0953-2048/29/4/045008>.
- <sup>11</sup> H. Wang, C. Dong, Q. Mao, R. Khan, X. Zhou, C. Li, B. Chen, J. Yang, Q. Su, and M. Fang, *Phys. Rev. Lett.* **111**, 207001 (2013), ISSN 0031-9007, URL <https://link.aps.org/doi/10.1103/PhysRevLett.111.207001>.
- <sup>12</sup> H. Lei, M. Abeykoon, K. Wang, E. S. Bozin, H. Ryu, D. Graf, J. B. Warren, and C. Petrovic, *J. Phys. Condens. Matter* **26**, 015701 (2014), ISSN 0953-8984, URL <https://iopscience.iop.org/article/10.1088/0953-8984/26/1/015701>.
- <sup>13</sup> J. Guo, S. Jin, G. Wang, S. Wang, K. Zhu, T. Zhou, M. He, and X. Chen, *Phys. Rev. B* **82**, 180520 (2010), ISSN 1098-0121, URL <https://link.aps.org/doi/10.1103/PhysRevB.82.180520>.
- <sup>14</sup> M. Fang, H. Wang, C. Dong, and Q. Huang, *J. Phys. Conf. Ser.* **449**, 012015 (2013), ISSN 1742-6596, URL <https://iopscience.iop.org/article/10.1088/1742-6596/449/1/012015>.
- <sup>15</sup> P. Dai, *Rev. Mod. Phys.* **87**, 855 (2015), ISSN 0034-6861, 1503.02340, URL <https://link.aps.org/doi/10.1103/RevModPhys.87.855>.
- <sup>16</sup> M. Wang, M. Yi, W. Tian, E. Bourret-Courchesne, and R. J. Birgeneau, *Phys. Rev. B* **93**, 075155 (2016), ISSN

- 2469-9950, 1508.04482, URL <https://link.aps.org/doi/10.1103/PhysRevB.93.075155>.
- 17 J. Yang, B. Chen, H. Wang, Q. Mao, M. Imai, K. Yoshimura, and M. Fang, *Phys. Rev. B* **88**, 064406 (2013), ISSN 1098-0121, URL <https://link.aps.org/doi/10.1103/PhysRevB.88.064406>.
  - 18 J. Huang, Z. Wang, H. Pang, H. Wu, H. Cao, S.-K. Mo, A. Rustagi, A. F. Kemper, M. Wang, M. Yi, et al., *Phys. Rev. B* **103**, 165105 (2021), ISSN 2469-9950, URL <https://link.aps.org/doi/10.1103/PhysRevB.103.165105>.
  - 19 Q. Fan, X. P. Shen, M. Y. Li, D. W. Shen, W. Li, X. M. Xie, Q. Q. Ge, Z. R. Ye, S. Y. Tan, X. H. Niu, et al., *Phys. Rev. B* **91**, 125113 (2015), ISSN 1098-0121, arXiv:1411.6455v1, URL <https://link.aps.org/doi/10.1103/PhysRevB.91.125113>.
  - 20 G. Kresse and J. Hafner, *Phys. Rev. B* **47**, 558 (1993), ISSN 0163-1829, URL <https://link.aps.org/doi/10.1103/PhysRevB.47.558>.
  - 21 A. Ehrlich and D. Rivier, *J. Phys. Chem. Solids* **29**, 1293 (1968), ISSN 00223697, URL <https://linkinghub.elsevier.com/retrieve/pii/0022369768901819>.
  - 22 A. E. Böhrer, V. Taufour, W. E. Straszheim, T. Wolf, and P. C. Canfield, *Phys. Rev. B* **94**, 024526 (2016), ISSN 2469-9950, 1606.00500, URL <https://link.aps.org/doi/10.1103/PhysRevB.94.024526>.
  - 23 J. G. Analytis, H.-h. Kuo, R. D. McDonald, M. Wartenbe, P. M. C. Rourke, N. E. Hussey, and I. R. Fisher, *Nat. Phys.* **10**, 194 (2014), ISSN 1745-2473, URL <http://dx.doi.org/10.1038/nphys2869http://www.nature.com/articles/nphys2869>.
  - 24 Q. Li, C. He, J. Si, X. Zhu, Y. Zhang, and H.-H. Wen, *Communications Materials* **1**, 16 (2020), ISSN 2662-4443, 1911.02420.
  - 25 J.-K. Bao, J.-Y. Liu, C.-W. Ma, Z.-H. Meng, Z.-T. Tang, Y.-L. Sun, H.-F. Zhai, H. Jiang, H. Bai, C.-M. Feng, et al., *Phys. Rev. X* **5**, 011013 (2015), ISSN 2160-3308, 1412.0067, URL <https://link.aps.org/doi/10.1103/PhysRevX.5.011013>.
  - 26 L. E. DeLong, R. P. Guertin, S. Hasanain, and T. Fariss, *Phys. Rev. B* **31**, 7059 (1985), ISSN 0163-1829, URL <https://link.aps.org/doi/10.1103/PhysRevB.31.7059>.
  - 27 K. Kadowaki and S. Woods, *Solid State Commun.* **58**, 507 (1986), ISSN 00381098, URL <https://linkinghub.elsevier.com/retrieve/pii/0038109886907854>.
  - 28 J. M. Daams and J. P. Carbotte, *J. Low Temp. Phys.* **43**, 263 (1981), ISSN 0022-2291, URL <http://link.springer.com/10.1007/BF00116155>.
  - 29 J. Bardeen, L. N. Cooper, and J. R. Schrieffer, *Phys. Rev.* **108**, 1175 (1957), ISSN 0031-899X, URL <https://www.taylorfrancis.com/books/9780429964251https://link.aps.org/doi/10.1103/PhysRev.108.1175>.
  - 30 W. L. McMillan, *Phys. Rev.* **167**, 331 (1968), ISSN 0031-899X, URL <https://link.aps.org/doi/10.1103/PhysRev.167.331>.
  - 31 A. Amon, E. Svanidze, R. Cardoso-Gil, M. N. Wilson, H. Rosner, M. Bobnar, W. Schnelle, J. W. Lynn, R. Gumeniuk, C. Hennig, et al., *Phys. Rev. B* **97**, 014501 (2018), ISSN 2469-9950, URL <https://link.aps.org/doi/10.1103/PhysRevB.97.014501>.
  - 32 M. Yi, Y. Zhang, Z. Shen, and D. Lu, *npj Quantum Materials* **2**, 57 (2017).
  - 33 F. Bouquet, Y. Wang, R. A. Fisher, D. G. Hinks, J. D. Jorgensen, A. Junod, and N. E. Phillips, *Europhys. Lett.* **56**, 856 (2001), ISSN 0295-5075, 0107196, URL <https://iopscience.iop.org/article/10.1209/epl/i2001-00598-7>.
  - 34 F. Bouquet, R. A. Fisher, N. E. Phillips, D. G. Hinks, and J. D. Jorgensen, *Phys. Rev. Lett.* **87**, 047001 (2001), ISSN 0031-9007, URL <https://link.aps.org/doi/10.1103/PhysRevLett.87.047001>.
  - 35 G. Xiao, Q. Zhu, Y. Cui, W. Yang, B. Li, S. Wu, G.-H. Cao, and Z. Ren, *Sci. China Physics, Mech. Astron.* **64**, 107411 (2021), ISSN 1674-7348, URL <https://link.springer.com/10.1007/s11433-021-1731-3>.